energies

MDPI

Article

# Estimation of Bearing Fault Severity in Line-Connected and Inverter-Fed Three-Phase Induction Motors

**Wagner Fontes Godoy [1], Daniel Morinigo-Sotelo [2], Oscar Duque-Perez [2,*], Ivan Nunes da Silva [3], Alessandro Goedtel [1] and Rodrigo Henrique Cunha Palácios [1]**

[1] Department of Electrical Engineering, Av. Alberto Carazzai, Federal Technological University of Paraná (UTFPR), 1640, Centro, Cornélio Procópio 86.300-000, PR, Brazil; wfgodoy@gmail.com (W.F.G.); agoedtel@utfpr.edu.br (A.G.); rodrigopalacios@utfpr.edu.br (R.H.C.P.)

[2] Department of Electrical Engineering, Paseo del Cauce, 59, University of Valladolid (UVa), 47011 Valladolid, Spain; daniel.morinigo@eii.uva.es

[3] Department of Electrical Engineering, University of São Paulo (USP), São Carlos School of Engineering, Av. Trabalhador São Carlense, 400, Centro, São Carlos 13.566-590, SP, Brazil; insilva@sc.usp.br

* Correspondence: oscar.duque@eii.uva.es

Received: 25 May 2020; Accepted: 30 June 2020; Published: 6 July 2020


**Abstract:** This paper addresses a comprehensive evaluation of a bearing fault evolution and its consequent prediction concerning the remaining useful life. The proper prediction of bearing faults in their early stage is a crucial factor for predictive maintenance and mainly for the production management schedule. The detection and estimation of the progressive evolution of a bearing fault are performed by monitoring the amplitude of the current signals at the time domain. Data gathered from line-fed and inverter-fed three-phase induction motors were used to validate the proposed approach. To assess classification accuracy and fault estimation, the models described in this paper are investigated by using Artificial Neural Networks models. The paper also provides process flowcharts and classification tables to present the prognostic models used to estimate the remaining useful life of a defective bearing. Experimental results confirmed the method robustness and provide an accurate diagnosis regardless of the bearing fault stage, motor speed, load level, and type of supply.

**Keywords:** three-phase induction motor; diagnosis; bearing faults; intelligent estimation

## 1. Introduction

Induction motors are widely used in industrial installations, playing a significant role in the production of components and accessories, given their features of robustness, cost, and reliability [1–3]. However, when operating under adverse conditions, these machines can develop electrical or mechanical faults in different parts such as stator, rotor, and bearings. Bearing faults are responsible for 40% to 90% of unexpected induction motors shutdowns [4–7]. These faults can be due to rotor asymmetries or to the bearing components (outer-race, inner-race, balls, or cage) [8,9]. In the case of inverter-fed motors, bearing faults can also be due to currents circulating through the bearings, which are caused by common voltage modes that induce currents in the shaft [10,11]. The development and evolution of bearing faults are mainly caused by adverse operating conditions: vibration, excessive load, shaft misalignment, eccentricity, corrosion, and incorrect assembly of the bearing on the shaft. Besides, inadequate lubrication can lead to bearing contamination, which is also an important factor of failure [1,12]. Hence, early-stage diagnosis of bearing faults is essential to increase process reliability.

The fault diagnosis has been addressed by monitoring different signals such as vibration, stator current or temperature, and implementing machine learning algorithms for automatic fault identification due to the relevance of this component in the fault context.

Vibration analysis is commonly applied to monitor bearing conditions [5]. In [13], the authors present a method for detecting vibration signals for bearing faults diagnosis, called bi-spectrum, based on empirical mode decomposition. In [14], the application of singular spectrum analysis is presented and differencing is used to denoise the signal and make it stationary. In considering null space pursuit and S transform strategies, time-frequency methods applied to bearing vibration signals are presented in [15]. In [3], the authors proposed the use of instantaneous frequency of motor voltage as a signal, and the global kurtosis as a measure of the defects. A microelectromechanical accelerometer to diagnose multiple bearing faults is used in [16]. In [17], spectral kurtosis is applied to select the optimal demodulation band in vibration signals containing high electromagnetic interference. This paper also compares the Fast Kurtogram and Protrugram approaches for the bearing inner and outer race fault diagnosis. In [1], the squared envelope spectrum analysis of the stator current, enhanced using spectral kurtosis algorithms, was performed to detect localized bearing faults. A method to diagnose bearing faults under the presence of gear noise using rotational order sideband identification is presented in [18]. Another approach for monitoring faults in low-speed bearings is proposed in [4], denoising the acoustic emission signal to improve the signal-to-noise ratio and applying an envelope analysis method to detect the periodic impacts due to bearing defects. Nevertheless, the use of the current instead of vibrations or noise has clear advantages, primarily related to the sensor used [1,6], but there are reported difficulties in using the stator current to detect these faults [19,20]. In [21], the authors propose a two-fold method that considers motor current signature analysis (MCSA) combined with infrared thermography data captured by a camera as additional data for condition monitoring. The combination of vibration and current signals is proposed in [22]. In [23], fast Fourier transform and the independent component analysis are applied to the current signal to diagnose bearing faults in inverter-fed motors. Reference [24] presents a review of signal processing techniques applied to bearing fault diagnosis.

The paper of reference [22] proposes a hybrid approach using vibration and electric signals. First, an anomaly is detected using only vibration data, and then the fault is classified with the hybrid approach. This work tested the bearing outer ring damage with 100% accuracy, using 50 data points for each test. Reference [25] compares four vibration analysis methods applied to the diagnosis of bearings implemented in low-power permanent magnet motors.

Strategies supported on intelligent systems are also applied in the identification of bearing faults [26]. Artificial Neural Networks (ANN) are among the most common methods used to classify machinery conditions [27]. Hence, through deep learning, deep neural networks with deep architectures are designed to mine useful information from raw data in order to diagnose bearing faults in rotating machines accurately. Through a combination of ANN, genetic algorithms, and wavelet analysis, the authors in [12] present the classification of the acoustic signal generated from a bearing under different levels of lubrication. In [28], a method is proposed for bearing fault diagnosis that is supported on feature extraction and selection, employing the adjusted distance discriminant technique and a selective ensemble of multiple fuzzy ARTMAP (Adaptive resonance theory mapping) algorithms. Reference [29] also uses a fuzzy ARTMAP algorithm, applying the Fourier–Bessel expansion to decompose the transient current signal into a series of single components. The authors of [30] focus on the use of fuzzy clustering for multi-fault bearing classification. Reference [31] combines probabilistic and simplified fuzzy neural networks to classify seven bearing states, using the energy entropy of the intrinsic mode functions of vibration signals, applying feature reduction. In [32], authors also use feature reduction via the principal component analysis, applied to bi-spectrum features, and determine the severity of the bearing failure with a support vector machine.

Reference [26] compares different machine learning and artificial intelligence techniques to detect minor bearing faults. Two different faults are considered: a hole and a scratch both practiced in the outer race of the bearing. Results indicate that support vector machines obtain the best results when

the number of classes into which it classifies is high. Nonetheless, neural networks are not tried in this paper. In [33], a multi-scale convolutional neural network is applied for bearing diagnosis using the vibration signals in the time domain. The diagnosis of the bearing condition is improved using a multi-attention mechanism. In [34], a method was proposed to predict a rolling bearing fault under different working conditions using vibration data. The methodology applies a neural network with backpropagation to classify the conditions; the neural network is optimized using the quantum particle swarm algorithm. A different neural network is implemented for each bearing of the motor, and the results of the networks are fused via the Dempster–Shafer evidence theory, which proposes using vibration signals.

This paper presents an alternative procedure to diagnose the progressive evolution of a bearing fault using the current signals in the time domain with the related advantages of the used sensor. The amplitudes of the signals are monitored directly using the half cycle of the waveform, which can be achieved with a low computational burden. Artificial Neural Networks are used to assess classification accuracy and fault estimation. Two complementary strategies are implemented to estimate the fault severity.

The contribution of this paper is given by the method employed to detect and estimate the progressive evolution of bearing faults in both line-connected and inverter-fed three-phase induction motors. No such estimation of bearing fault evolution has been reported in the researched literature. A case study is presented with 840 experimental tests performed on a 1 hp motor, in steady-state, using different supplies (utility supply and two frequency inverters, with an operating frequency between 25 and 75 Hz) and under different switching frequencies and load conditions. Results show that the estimation of bearing fault evolution can be properly addressed.

Finally, obtained results are compared with previously published techniques that consider the use of transforms, vibration analysis, and other MCSA based techniques. The estimation of the evolution of a bearing fault proposed in this work assists the operator in decision-making, providing the effectiveness of strategic maintenance planning and the consequent increase in the availability of machines and processes.

This paper is organized as follows: Section 2 presents the proposed methodology for fault diagnosis. Section 3 presents experimental data results and comparison with previous works, while the conclusions are shown in Section 4.

## 2. Methodology

This section presents the methodological approach employed in the development of this research.

Experimental data are gathered by directly sampling the three-phase stator current signals in the time domain. Figure 1 shows the process flow chart for the proposed diagnosis approach. During the data preprocessing step, one of the half-cycles per each phase current is randomly chosen to represent each performed test. Figure 2 shows how each half-cycle of the signal is represented by 50 values, sequentially extracted, following the method presented in [35], and representing the necessary information for the classifier without mischaracterizing the original waveform.

The next step is data normalization, which is performed by dividing the values of each waveform by the largest one, ensuring that no influence of load or frequency level will impact classification results. The data are randomly fed to the classification algorithms, ensuring that the created input vector represents the entire waveform domain. The discretized current signals of Figure 2 are shown normalized [36].

After signal preprocessing, the first stage of classification carries out a preliminary diagnosis (defective/non-defective motor). In case a bearing failure is identified, the samples are subjected to the verification of its severity, using two different strategies:

- Strategy 1: This strategy classifies up to four predefined patterns representing qualitative ranges of severity, where level 1 represents first bearing wear, level 2 considers moderate wear, and level 3 represents an advanced failure. Finally, level 4 considers a bearing operating at critical conditions.

- Strategy 2: An estimator performs a functional approximation, identifying up to ten levels of severity, in which levels 1 and 10 represent the most initial degradation level of a fault evolving to the most critical situation, respectively.

To perform the classifications, neural networks are used, which are a set of connected input/output units. The task is performed by associating a weight to each connection and adjusting it in a training phase [37,38]. A neural network derives its maximum computing potential through its structure and its ability to learn and generalize [38]. Multilayer Perceptron (MLP) has been chosen among neural networks since several works have proven its validity for electric motor diagnosis [28,29,32,35,36]. For training the network, backpropagation (as explained in [34]) with the momentum learning rule is used. Weights matrices were initiated with random values, and the learning rate parameter was defined as $\eta = 0.2$ and precision as $\varepsilon = 10^6$. The hyperbolic tangent function is used to activate the hidden layer. The neural network is structured in three layers, with 150 inputs, 76 neurons in the intermediate layer, one neuron in the output layer when the network is performing as a single classifier, and four neurons for multiclassification performance.

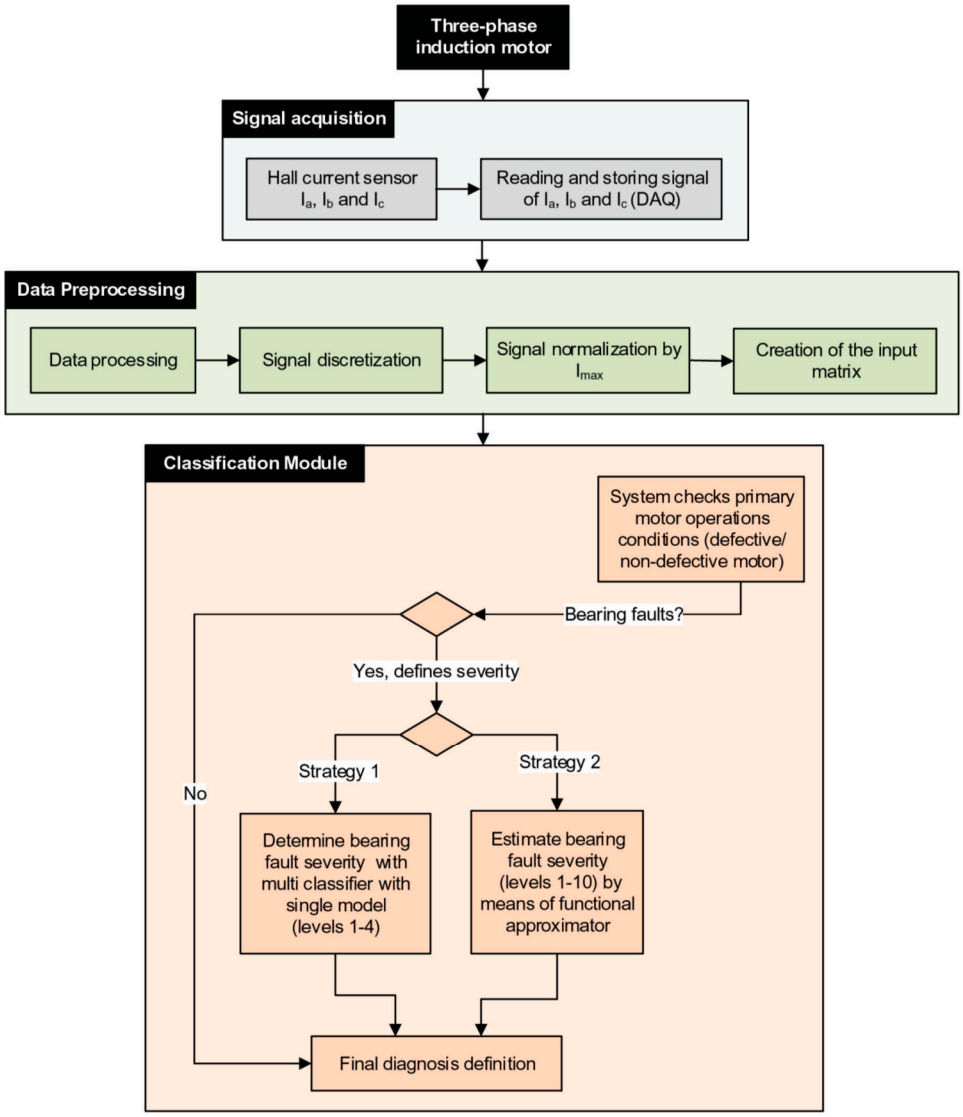


**Figure 1.** The functionality of the proposed diagnostic system.

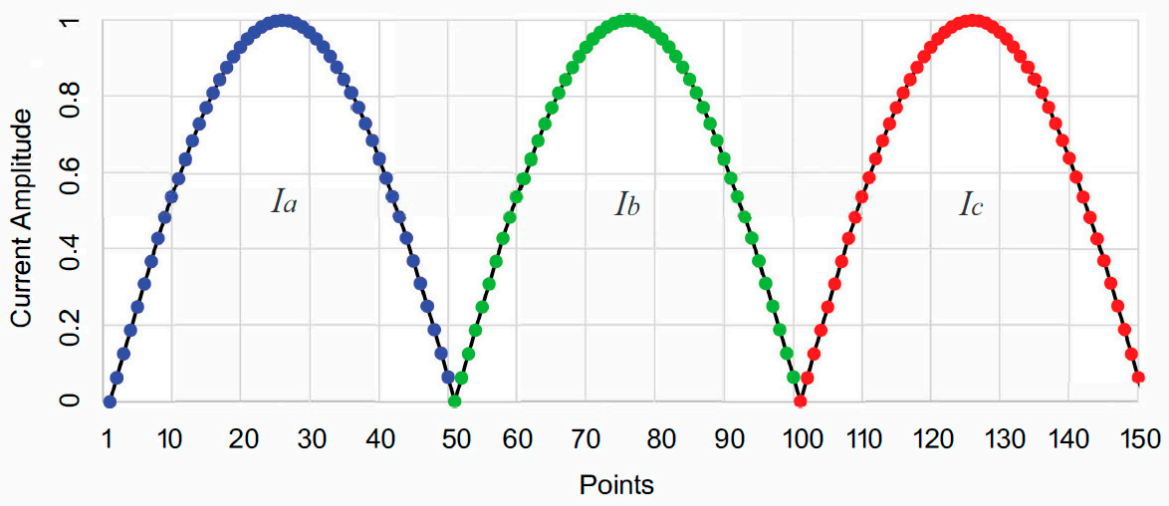


**Figure 2.** Input data modeling: current discretization and normalization.

## 3. Case Study

### *3.1. Test Bench*

This work considers the progressive evolution of bearing wear caused by the contamination of the lubrication during assembly. This procedure seeks similarity to the natural wear process caused due to the excessive use and inadequate lubrication. These situations are commonly found in the industrial environment.

The test bench is shown in Figure 3. The motor was star-connected, with a voltage supply of 400 V. The motor is loaded with a Telemecanic magnetic brake directly coupled to the machine shaft. The motor has been tested under four different supplies: direct-line supply and three inverters (Allen Bradley—Power Flex 40 or WEG—CFW08 Plus) working under open-loop V/Hz control. Different switching frequencies (4 and 5 kHz) and operating frequencies (from 25 to 75 Hz) were considered. The case study has been designed to validate the proposed methodology for different models and the modes of operation of inverters commercially available.

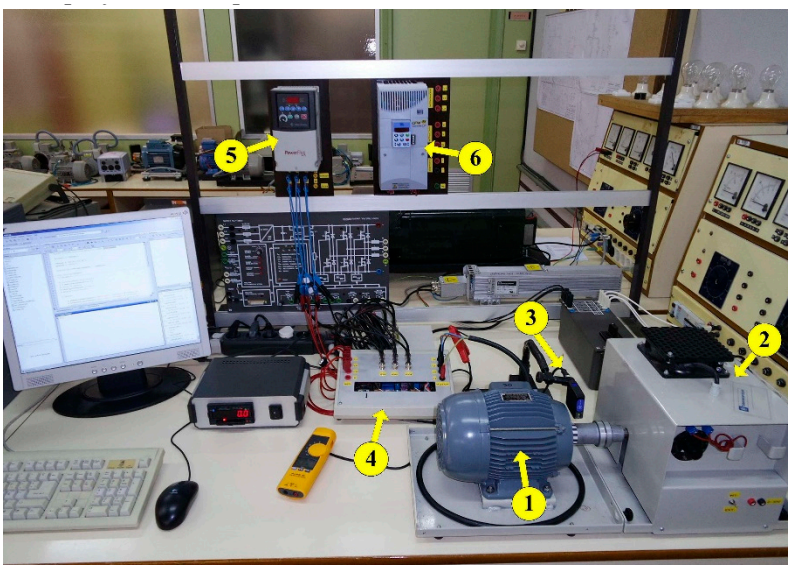


**Figure 3.** Experimental workbench: (1) Induction motor, (2) magnetic brake, (3) Optical sensor, (4) Data acquisition board, (5) Allen Bradley, and (6) WEG inverters.

Hall effect sensors (LEM) and a DAC PCI-6250 M model (16 analog inputs—16-bit 1 MS/s) of National Instruments (TM) are employed to collect data. The acquisition rate for all tests was 25 kHz with an acquisition time of 25 s, capturing from startup to steady-state. For speed measure, a Datalogic optical sensor model S60-PA-5-W08-NH was used. A single row bearing model SKF Explorer 6004 was employed, with specifications as described in Table 1.

**Table 1.** SKF Explorer 6004 Bearing specifications.

| Parameters | Specifications |
|---|---|
| Hole diameter (mm) | 20 |
| External diameter (mm) | 42 |
| Width (mm) | 12 |
| Dynamic load (kN) | 9.95 |
| Static load (kN) | 5 |
| Reference speed (r/min) | 38,000 |
| Limit speed (r/min) | 24,000 |

Table 2 describes the adopted conditions for each test. For each supply, 40 samples were collected while considering bearing at healthy conditions (20 samples for the motor running with no load and 20 samples for the motor operating with the rated load), and 100 samples were collected for the motor operating at defective condition (50 samples for the motor operating with no load and more than 50 samples for the motor running with the rated load).

**Table 2.** Description of test conditions.

| | Supply | Frequency | Switching Frequency | Bearing Condition | Nº of Acquisitions |
|---|---|---|---|---|---|
| 1 | Allen Bradley | 50 Hz | 4 kHz | Healthy | 40 |
| | | | | Faulty | 100 |
| 2 | Allen Bradley | 25 Hz | 4 kHz | Healthy | 40 |
| | | | | Faulty | 100 |
| 3 | Allen Bradley | 75 Hz | 4 kHz | Healthy | 40 |
| | | | | Faulty | 100 |
| 4 | Allen Bradley | 50 Hz | 5 kHz | Healthy | 40 |
| | | | | Faulty | 100 |
| 5 | WEG | 50 Hz | 5 kHz | Healthy | 40 |
| | | | | Faulty | 100 |
| 6 | Line-fed | 50 Hz | | Healthy | 40 |
| | | | | Faulty | 100 |

The replacement of bearings to simulate or create fault conditions is a widely used technique [1], but anytime the motor is disassembled, reassembled, and realigned, the test conditions change. To avoid the replacement, the health conditions were obtained using a new set of bearings, and the faulty conditions were created by contaminating the grease of the front bearings with silicon carbide (SiC), as shown in Figure 4. Silicon carbide ceramics have high corrosion and erosion stability, and high thermal conductivity.

According to [32], the process of bearing degradation is very complex, especially the process of natural degradation. Thus, gradual contamination of the bearing grease with SiC was performed, aiming to estimate the gradual evolution of the bearing degradation over time.

After first contaminating the bearing grease, five samples were collected for each of the supplies. These tests represent an incipient bearing fault. Then, to force the wearing of the bearing, the motor was run uninterruptedly for 12 h, with no load and line-fed.

In addition to the currents, the temperature was also monitored. After complete motor cooling, new acquisitions for each of the test conditions were performed. This procedure was repeated for 9 days until the bearing block occurred. Each interval of this sequence of tests was defined as a specific degree of evolution of the bearing degradation.

Figure 5 shows the bearing after the tests. The bearing deterioration is visually noticeable due to the significant presence of steel chips (internal/external rings as well as in the balls), a characteristic similar to that observed in those parts with excessive wear, high time of operation, or lack of lubrication.

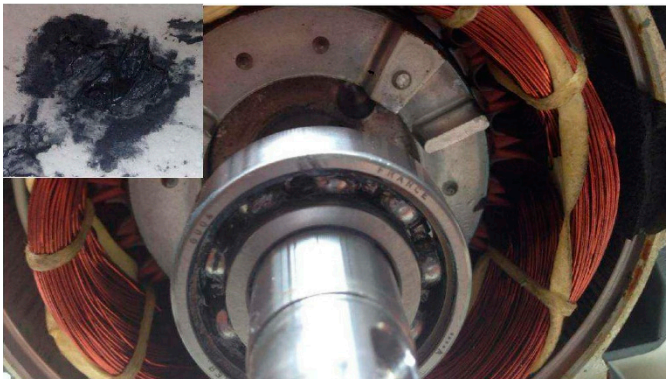

**Figure 4.** Bearing contamination with silicon carbide (SiC).

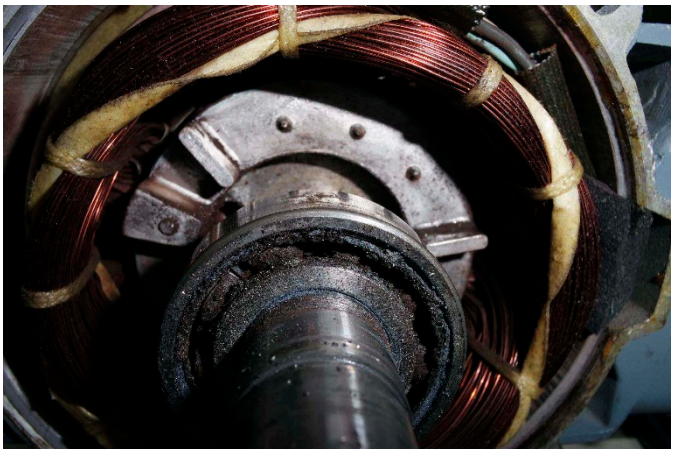

**Figure 5.** Bearing wear after the test run.

### 3.2. Experimental Results

First, results concerning the bearing condition (defective/healthy) are presented, followed by the results related to the determination of the bearing fault level and, finally, the estimation of the bearing fault severity.

The first stage of classification is to check and carry out the primary diagnosis (healthy/defective bearing condition). If the bearing is healthy, the system performs the final diagnosis directly. In the case of the detection of a bearing defect, the system performs the determination of the bearing fault level. Table 3 shows the results obtained with the first stage of the proposed methodology and compares the performance for line-fed and inverter-fed tests.

The accuracy measures the classifier's success by dividing the number of correct classifications by the number of total samples. The mean absolute error measures how far the misclassification samples are from the actual ones, while the relative absolute error is obtained by dividing the mean absolute error by the module of the actual value.

Table 3 shows that classification accuracy exceeds 98% for the line-supplied motor. The Kappa index is higher than 0.80, which confirms the capability of the generalization of the proposed strategy. By applying the same considerations to the tests performed with the same motor driven by different inverters, an accuracy of 81.96% was reached. The precision to classify the motor operating under defective conditions in case of a line-fed motor is 99%, while for an inverter-fed motor, it is 87%.

The area under the ROC curve (receiver operating characteristic curve) reflects the overall accuracy of the method, and it depends on how precise the groups are separated into those with and without fault.

**Table 3.** Fault classification—motor operation under healthy/defective conditions.

| Attributes | Line Connected | | Inverter-Fed Supply | |
|---|---|---|---|---|
| Correctly classified instances (%) | 98.6 | | 81.96 | |
| Incorrectly classified instances (%) | 1.39 | | 18.04 | |
| Kappa statistic | 0.97 | | 0.58 | |
| Mean absolute error | 0.01 | | 0.18 | |
| Root mean squared error | 0.10 | | 0.37 | |
| Relative absolute error (%) | 4.92 | | 44.65 | |
| Root relative squared error (%) | 23.74 | | 80.49 | |
| Detailed accuracy by class | Healthy | Defective | Healthy | Defective |
| TP rate [1] | 0.97 | 0.99 | 0.70 | 0.87 |
| FP rate [2] | 0.01 | 0.02 | 0.12 | 0.29 |
| Precision | 0.97 | 0.99 | 0.71 | 0.87 |
| Recall | 0.97 | 0.99 | 0.70 | 0.87 |
| F measure | 0.97 | 0.99 | 0.70 | 0.87 |
| MCC [3] | 0.97 | 0.97 | 0.57 | 0.57 |
| ROC [4] | 0.99 | 0.99 | 0.90 | 0.90 |
| Area | 0.99 | 1.00 | 0.82 | 0.95 |

[1] True Positives rate; [2] False Positives rate; [3] Matthews Correlation Coefficient; [4] Receiver Operating Characteristic curve.

TP rate of true positives indicates the number of instances correctly classified as a given class, and the FP rate of false positives indicates the number of instances falsely classified as a given class. In both scenarios, a reduction in false negatives and a slight increase in false positives are observed.

The MCC (Matthews correlation coefficient) shows the right prediction for both scenarios. This score is generally considered as a good way to measure binary classifications, even when the two classes are of different sizes.

As expected, the different inverter-fed motor scenarios present an accuracy slightly lower than for the line-fed motor, as shown in the confusion matrix of Table 4.

**Table 4.** Confusion matrix.

| | Predict Classes | | | |
|---|---|---|---|---|
| | Line-connected | | Inverter-fed | |
| Classes | Healthy | Defective | Healthy | Defective |
| Healthy | 36 | 1 | 124 | 53 |
| Defective | 1 | 105 | 50 | 344 |

As previously explained, when a bearing failure is identified, the samples are subjected to the verification of its severity, as follows.

### *3.3. Strategy 1—Determination of Bearing Fault Level*

As explained in Section 2, this strategy considers the use of an MLP Network that classifies up to four predefined patterns representing qualitative ranges of severity. Tests carried out after the first contamination have been assigned to deterioration level 1. The previously defined contamination process, running the engine for 12 h without load and performing the tests, was repeated for 10 days. The tests on days 2, 3, and 4 correspond to level 2; those on days 5, 6, and 7 to level 3; and the tests of the last 3 days to level 4, equivalent to critical conditions.

Table 5 presents the classification results for the different levels of bearing defect. It is noticed that the line-fed motor's classification results reached accuracy rates up to 93.13%, and the inverter-fed

tests achieved an accuracy of 80.22%. It is also observed that the Kappa index, precision, and other statistical measures obtained by the tests performed for the line-fed motor indicate excellent results.

**Table 5.** Multiclassification.

| **Attributes** | **Line Connected** | | | | **Inverter-Fed Supply** | | | |
|---|---|---|---|---|---|---|---|---|
| Correctly classified instances (%) | 93.13 | | | | 80.22 | | | |
| Incorrectly classified instances (%) | 6.86 | | | | 19.77 | | | |
| Kappa statistic | 0.90 | | | | 0.73 | | | |
| Mean absolute error | 0.06 | | | | 0.10 | | | |
| Root mean squared error | 0.19 | | | | 0.28 | | | |
| Relative absolute error (%) | 16.93 | | | | 29.04 | | | |
| Root relative squared error (%) | 43.06 | | | | 66.09 | | | |
| Detailed accuracy by class | Level 1 | Level 2 | Level 3 | Level 4 | Level 1 | Level 2 | Level 3 | Level 4 |
| TP rate [1] | 0.83 | 0.96 | 0.96 | 0.96 | 0.72 | 0.82 | 0.83 | 0.83 |
| FP rate [2] | 0.01 | 0.08 | 0.00 | 0.00 | 0.04 | 0.10 | 0.09 | 0.03 |
| Precision | 0.95 | 0.81 | 1.00 | 1.00 | 0.83 | 0.76 | 0.79 | 0.84 |
| Recall | 0.83 | 0.96 | 0.96 | 0.95 | 0.72 | 0.81 | 0.83 | 0.83 |
| F measure | 0.88 | 0.88 | 0.98 | 0.97 | 0.77 | 0.79 | 0.81 | 0.84 |
| MCC [3] | 0.86 | 0.84 | 0.97 | 0.97 | 0.72 | 0.70 | 0.72 | 0.81 |
| ROC [4] | 0.95 | 0.95 | 1.00 | 0.99 | 0.93 | 0.90 | 0.93 | 0.94 |
| Area | 0.87 | 0.91 | 1.00 | 0.99 | 0.85 | 0.85 | 0.86 | 0.87 |

[1] True Positives rate; [2] False Positives rate; [3] Matthews Correlation Coefficient; [4] Receiver Operating Characteristic curve.

The precision of the tests performed with the inverter-fed motor presents the following rates: 83%, 76%, 79%, and 84% for the motor operating with different bearing fault levels. MCC and ROC statistics present excellent results. The confusion matrix shown in Table 6 clearly distinguishes and classifies the different bearing faulty levels.

**Table 6.** Confusion matrix.

| **Predicted Classes** | | | | |
|---|---|---|---|---|
| | Line-connected | | | |
| Classes | Level 1 | Level 2 | Level 3 | Level 4 |
| Level 1 | 20 | 4 | 0 | 0 |
| Level 2 | 1 | 27 | 0 | 0 |
| Level 3 | 0 | 1 | 28 | 0 |
| Level 4 | 0 | 1 | 0 | 20 |
| | Inverter-fed | | | |
| Classes | Level 1 | Level 2 | Level 3 | Level 4 |
| Level 1 | 97 | 23 | 14 | 0 |
| Level 2 | 15 | 148 | 14 | 4 |
| Level 3 | 3 | 18 | 157 | 12 |
| Level 4 | 1 | 4 | 13 | 89 |

Figures 6 and 7 present the distribution chart considering each level of bearing fault under evaluation in this work. It can be seen that there is a proportional distribution for the faults under evaluation, where each color represents a specific faulty level.

### *3.4. Strategy 2—Estimation of Bearing Fault Severity*

Finally, the estimation of the bearing wear severity level is proposed to assist the operator in the process of decision-making, providing the effectiveness of correct strategic planning for maintenance and the consequent increase of the availability of machines and processes.

Following a criterion similar to that adopted for the determination of the bearing fault level, in this scenario, the sets of samples representing each of the 10 days of tests were defined in a scale (1–10), representing the progressive evolution of the bearing wear. The wear evolves from an incipient defect,

followed by an intermediate and an advanced one until reaching a critical level (ninth and tenth days of testing), where the bearing's immediate replacement is necessary to maintain the process integrity.

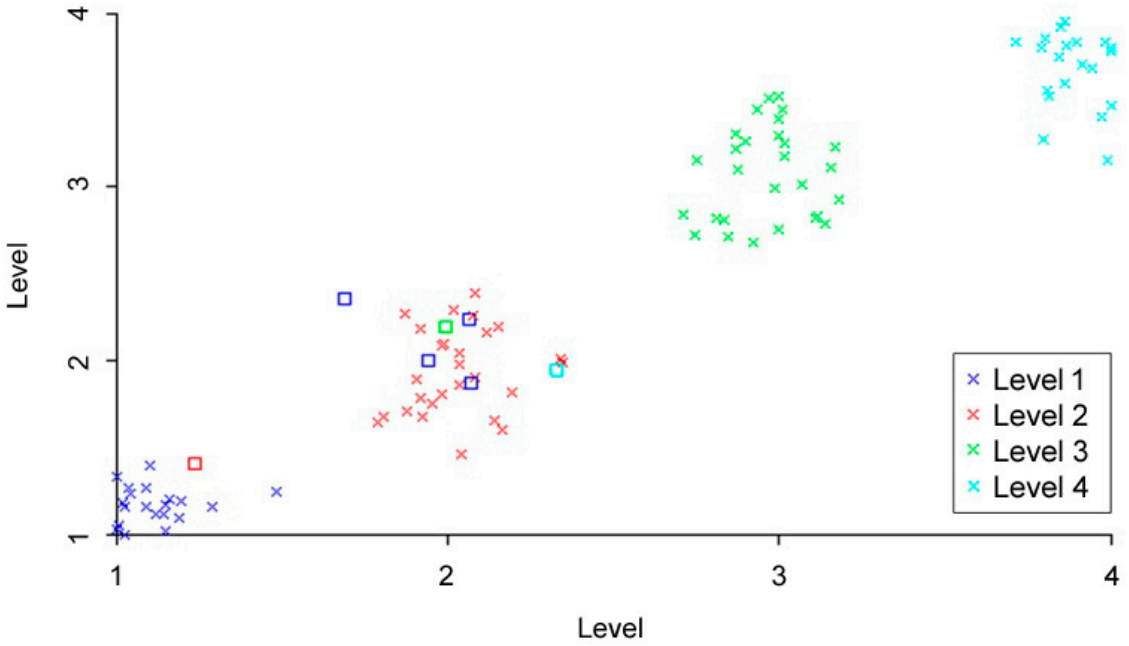


**Figure 6.** Faulty distribution chart—Line-fed motor.

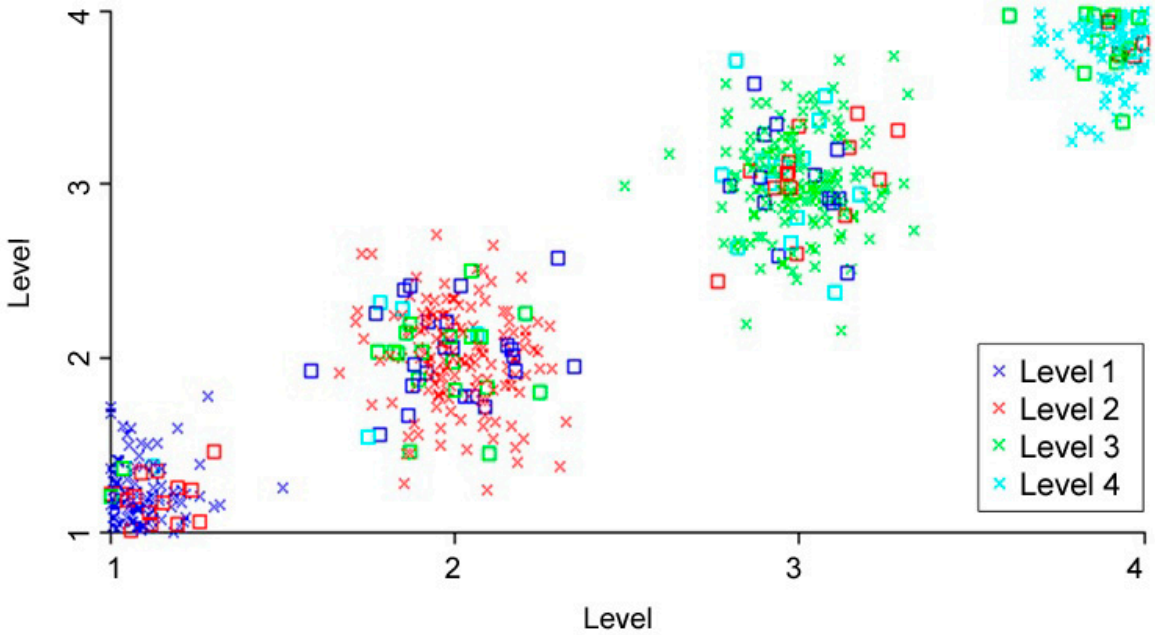


**Figure 7.** Faulty distribution chart—Inverter-fed motor.

Figures 8 and 9 show the results of the estimation of the progressive bearing wear evolution caused after performing an incorrect lubrication procedure. Axis y shows the wear level as a function of the number of days (normalized), and axis x represents the number of validation samples.

The results obtained from the validation test were promising since, in general, the mean relative error was 45.34%, and the error variance was −2.13%. It has to be taken into account the complexity of the problem addressed and the fact that different models of frequency inverters, under variable speed ranges, switching frequencies, and different load levels, were considered.

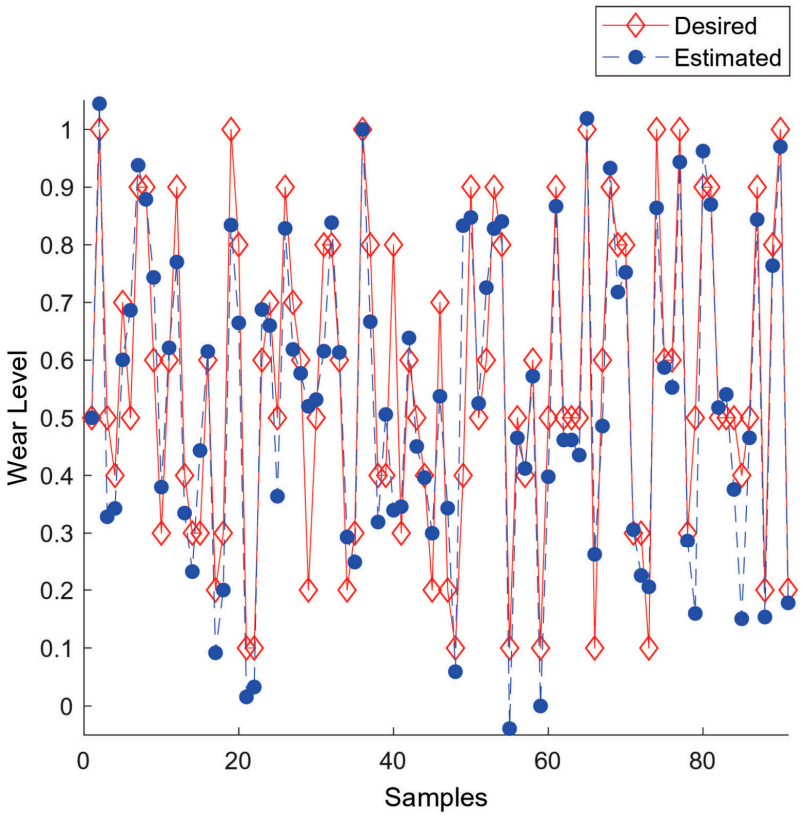


**Figure 8.** Neural estimator—wear evolution of a bearing fault—Line connect.

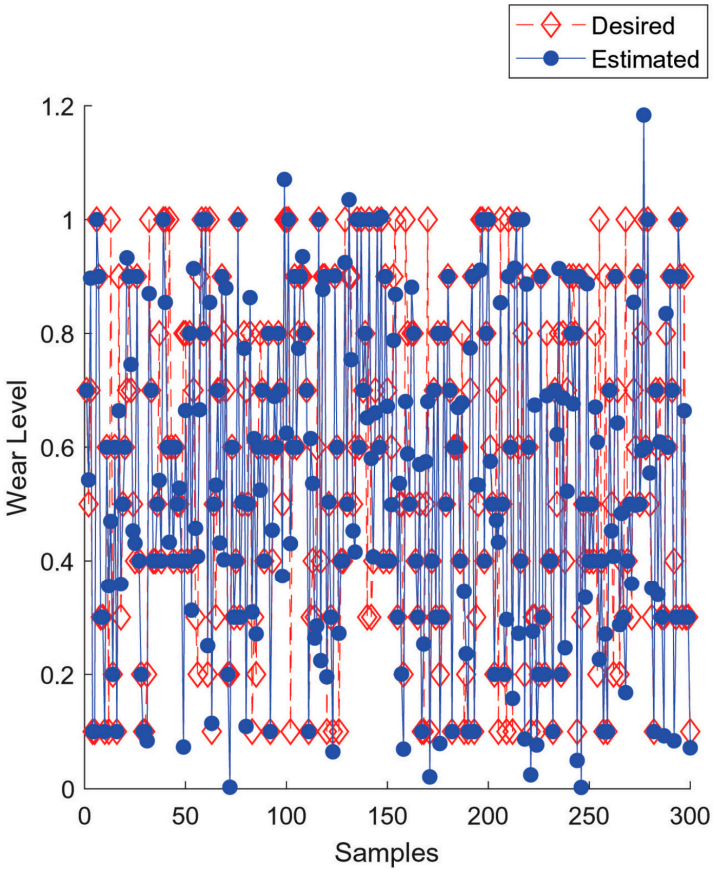


**Figure 9.** Neural estimator—wear evolution of a bearing fault—Inverter-fed.

In the case of the line-fed motor, an average relative error of 16.36% and an error variance of −3.96% were obtained. These results prove the efficiency of the proposed methodology of fault insertion, and mainly the estimation of the bearing wear evolution studied in this work.

### *3.5. Comparison with Some Previous Research*

In this work, an effort is made to characterize the estimation of the evolution of a bearing fault. The experimental setup considers different supply conditions and collects current signals taken from different bearing degradation conditions under different speed and torque conditions.

Another critical point is that this work considers the use of two different classification strategies for the diagnosis of failures, while other works employ a single tool. Also, this work considers the use of different models of frequency inverters, operating with different switching frequencies, while other studies employ a single inverter, except for [39,40], which consider the use of two inverters. Besides, it was possible to evaluate machine fault behavior under different frequencies and load levels. According to the literature, frequency variation is considered only in [16,41–44]. A wide variation of the load is already presented in [16,45].

Exclusively considering bearing faults, the contribution of this work refers to the use of discrete current signals in the time domain to classify the progressive evolution of defects caused by the contamination of the lubrication during assembly. At the same time, the literature shows results based on the creation of artificial faults [42–47]. The application of traditional methods that consider the temperature and vibration monitoring to classify bearing conditions has also been considered [32,46,48]. The cost of vibration monitoring sensors associated with signal processing devices restricts their use in industrial environments in general.

Finally, in this work, the concept of multiclassification and the estimation of the fault severity level were introduced. The sets of samples representing each test were separated into scales following the development from an incipient fault, followed by an intermediate class of fault, and evolving into advanced failure until it reaches a critical level where immediate replacement of the damaged bearing is required. The literature consulted presents a similar concept of the evaluation of the severity of bearing failures only for the diagnosis of line-fed machines [32,34,49]. The results obtained in this work can be used as a support tool to allow efficient scheduling of a planned process interruption, providing the application of this strategy at real-time monitoring conditions.

The Classification Learner app from Matlab 2017b has been used to compare the results with algorithms already applied and published in this field. The amplitudes of the fault frequencies resulting from the common application of MCSA have been used as inputs (faults associated with outer race, inner race, bearing balls, and cage faults) [12]. Five-fold cross-validation has been considered to train and evaluate the available classifiers in the mentioned app. For the binary classification, the best accuracy is obtained for the line-fed motor at a nominal load using linear discriminant and logistic regression (86.7%); the next best results are obtained with the quadratic discriminant and the medium Gaussian Support Vector Machines (83.3% of accuracy). In other cases (inverter-fed motor at no load), the results are much worse. For the case of multiclassification, the best results are also obtained for the line-fed motor at nominal load. However, in this case, the best performance is achieved using Quadratic SVM (with an accuracy of just 47.1%). Also, the multiclassification results are much worse for the rest of the operating conditions, showing that the proposed methodology outperforms these known methods.

## 4. Conclusions

This paper has presented a novel procedure to diagnose the progressive evolution of a bearing fault using the current signals directly in the time domain. The validity and effectiveness of the proposed method are verified through the simulation of a bearing accelerated life test under laboratory conditions. The methodology analyzes the amplitude of the current signal in a semicycle of the three-line currents. These data are then presented directly as input to the pattern classifier; therefore, the procedure does

not require the complete cycle or n cycles, as in the case of fast Fourier transform, making it faster and with less computational cost.

The experimental data were collected from a motor-driven by different models of frequency inverters with different operating frequencies, switching frequencies, and load levels. The results show that the proposed approach is immune to speed or load variations in the machine shaft, proving its effectiveness.

The major challenge faced in this work has been related to the proper identification of minor incipient faults in inverter-fed induction motors.

Different levels of bearing fault evolution are classified by using an MLP network, achieving precision rates of more than 97% for the line-fed motor, and more than 71% for the inverter-fed machines. As highlighted earlier, the novelty of the present contribution lies in identifying an incipient fault evolution with a focus on remaining bearing life as a support tool for practical application in real-time monitoring conditions.

Correct fault identification improves machine reliability and reduces maintenance costs. Thus, in this work, the development of a fault detection system was proposed, based on data collected by current sensors, usually available in the industry, allowing for the proper diagnosis of electrical and mechanical failures of the machine.

**Author Contributions:** Conceptualization, W.F.G., A.G., O.D.-P., and D.M.-S.; Data curation, W.F.G.; Methodology, W.F.G., I.N.d.S., A.G.; Software W.F.G., A.G., O.D.-P., and R.H.C.P.; Validation, D.M.-S., R.H.C.P.; Writing—original draft, W.F.G., A.G., O.D.-P., and D.M.-S.; Writing—review & editing, A.G. and O.D.-P. All authors have read and agreed to the published version of the manuscript.

**Funding:** This research was funded by CAPES (process BEX552269/2011-5) and National Council for Scientific and Technological Development (CNPq) under grant #474290/2008-3, #473576/2011-2, #552269/2011-5, #307220/2016-8.

**Acknowledgments:** The authors gratefully acknowledge the contributions of Universities of Valladolid and Federal Technological University of Paraná for their financial support toward the development of this research. The authors are also grateful to WEG Iberia for the donation of one of the inverters used in this work.

**Conflicts of Interest:** The authors declare no conflict of interest.

## References

1. Leite, V.C.M.N.; da Silva, J.G.B.; Veloso, G.F.C.; da Silva, L.E.B.; Lambert-Torres, G.; Bonaldi, E.L.; de Oliveira, L.E.L. Detection of localized bearing faults in induction machines by spectral kurtosis and envelope analysis of stator current. *IEEE Trans. Ind. Electron.* **2015**, *62*, 1855–1865. [CrossRef]
2. Wang, Z.; Yang, J.; Li, H.; Zhen, D.; Xu, Y.; Gu, F. Fault identification of broken rotor bars in induction motors using an improved cyclic modulation spectral analysis. *Energies* **2019**, *12*, 3279. [CrossRef]
3. Dalvand, F.; Kalantar, A.; Safizadeh, M.S. A novel bearing condition monitoring method in induction motors based on instantaneous frequency of motor voltage. *IEEE Trans. Ind. Electron.* **2016**, *63*, 364–376. [CrossRef]
4. Kang, M.; Kim, J.; Kim, J.M. High-performance and energy-efficient fault diagnosis using effective envelope analysis and denoising on a general-purpose graphics processing unit. *IEEE Trans. Power Electron.* **2015**, *30*, 2763–2776. [CrossRef]
5. Riera-Guasp, M.; Antonino-Daviu, J.A.; Capolino, G.A. Advances in electrical machine, power electronic, and drive condition monitoring and fault detection: State of the art. *IEEE Trans. Ind. Electron.* **2015**, *62*, 1746–1759. [CrossRef]
6. Bellini, A.; Filippetti, F.; Tassoni, C.; Capolino, G.A. Advances in diagnostic techniques for induction machines. *IEEE Trans. Ind. Electron.* **2008**, *55*, 4109–4126. [CrossRef]
7. Toma, R.N.; Prosvirin, A.E.; Kim, J.M. Bearing fault diagnosis of induction motors using a genetic algorithm and machine learning classifiers. *Sensors* **2020**, *20*, 1884. [CrossRef] [PubMed]
8. Muetze, A.; Binder, A. Practical rules for assessment of inverter-induced bearing currents in inverter-fed ac motors up to 500 kW. *IEEE Trans. Ind. Electron.* **2007**, *54*, 1614–1622. [CrossRef]
9. Mishra, C.; Samantaray, A.; Chakraborty, G. Rolling element bearing defect diagnosis under variable speed operation through angle synchronous averaging of wavelet de-noised estimate. *Mech. Syst. Signal Process.* **2016**, *72–73*, 206–222. [CrossRef]

10. Prudhom, A.; Antonino-Daviu, J.A.; Razik, H.; Climente-Alarcon, V. Time-frequency vibration analysis for the detection of motor damages caused by bearing currents. *Mech. Syst. Signal Process.* **2017**, *84*, 747–762. [CrossRef]
11. Ren, X.; Liu, R.; Yang, E. Modelling of the bearing breakdown resistance in bearing currents problem of AC motors. *Energies* **2019**, *12*, 1121. [CrossRef]
12. Sadegh, H.; Mehdi, A.N.; Mehdi, A. Classification of acoustic emission signals generated from journal bearing at different lubrication conditions based on wavelet analysis in combination with artificial neural network and genetic algorithm. *Tribol. Int.* **2016**, *95*, 426–434. [CrossRef]
13. Saidi, L.; Ali, J.B.; Fnaiech, F. Bi-spectrum based-EMD applied to the non-stationary vibration signals for bearing faults diagnosis. *ISA Trans.* **2014**, *53*, 1650–1660. [CrossRef] [PubMed]
14. Al-Bugharbee, H.; Trendafilova, I. A fault diagnosis methodology for rolling element bearings based on advanced signal pretreatment and autoregressive modelling. *J. Sound Vib.* **2016**, *369*, 246–265. [CrossRef]
15. Zhu, D.; Gao, Q.; Sun, D.; Lu, Y.; Peng, S. A detection method for bearing faults using null space pursuit and S transform. *Signal Process.* **2014**, *96*, 80–89. [CrossRef]
16. Maruthi, G.S.; Hegde, V. Application of MEMS Accelerometer for Detection and Diagnosis of Multiple Faults in the Roller Element Bearings of Three Phase Induction Motor. *IEEE Sens. J.* **2016**, *16*, 145–152. [CrossRef]
17. Smith, W.A.; Fan, Z.; Peng, Z.; Li, H.; Randall, R.B. Optimised Spectral Kurtosis for bearing diagnostics under electromagnetic interference. *Mech. Syst. Signal Process.* **2016**, *75*, 371–394. [CrossRef]
18. Wang, T.; Liang, M.; Li, J.; Cheng, W.; Li, C. Bearing fault diagnosis under unknown variable speed via gear noise cancellation and rotational order sideband identification. *Mech. Syst. Signal Process.* **2015**, *62*, 30–53. [CrossRef]
19. Immovilli, F.; Bellini, A.; Rubini, R.; Tassoni, C. Diagnosis of bearing faults in induction machines by vibration or current signals: A critical comparison. *IEEE Trans. Ind. Appl.* **2010**, *46*, 1350–1359. [CrossRef]
20. Blodt, M.; Granjon, P.; Raison, B.; Rostaing, G. Models for bearing damage detection in induction motors using stator current monitoring. *IEEE Trans. Ind. Electron.* **2008**, *55*, 1813–1822. [CrossRef]
21. Picazo-Ródenas, M.J.; Antonino-Daviu, J.; Climente-Alarcon, V.; Royo-Pastor, R.; Mota-Villar, A. Combination of noninvasive approaches for general assessment of induction motors. *IEEE Trans. Ind. Appl.* **2015**, *51*, 2172–2180. [CrossRef]
22. Chang, H.-C.; Jheng, Y.-M.; Kuo, C.-C.; Hsueh, Y.-M. Induction motors condition monitoring system with fault diagnosis using a hybrid approach. *Energies* **2019**, *12*, 1471. [CrossRef]
23. Yang, T.; Pen, H.; Wang, Z.; Chang, C.S. Feature knowledge based fault detection of induction motors through the analysis of stator current data. *IEEE Trans. Instrum. Meas.* **2016**, *65*, 549–558. [CrossRef]
24. Rai, A.; Upadhyay, S. A review on signal processing techniques utilized in the fault diagnosis of rolling element bearings. *Tribol. Int.* **2016**, *96*, 289–306. [CrossRef]
25. Skora, M.M.; Ewert, P.; Kowalski, C.T. Selected rolling bearing fault diagnostic methods in wheel embedded permanent magnet brushless direct current motors. *Energies* **2019**, *12*, 4212. [CrossRef]
26. Esakimuthu Pandarakone, S.; Mizuno, Y.; Nakamura, H. A Comparative study between machine learning algorithm and artificial intelligence neural network in detecting minor bearing fault of induction motors. *Energies* **2019**, *12*, 2105. [CrossRef]
27. Jia, F.; Lei, Y.; Lin, J.; Zhou, X.; Lu, N. Deep neural networks: A promising tool for fault characteristic mining and intelligent diagnosis of rotating machinery with massive data. *Mech. Syst. Signal Process.* **2016**, *72*, 303–315. [CrossRef]
28. Xu, Z.; Li, Y.; Wang, Z.; Xuan, J. A selective fuzzy {ARTMAP} ensemble and its application to the fault diagnosis of rolling element bearing. *Neurocomputing* **2016**, *182*, 25–35. [CrossRef]
29. Tran, V.T.; AlThobiani, F.; Ball, A.; Choi, B.K. An application to transient current signal based induction motor fault diagnosis of Fourier Bessel expansion and simplified fuzzy ARTMAP. *Expert Syst. Appl.* **2013**, *40*, 5372–5384. [CrossRef]
30. Li, C.; de Oliveira, J.V.; Cerrada, M.; Pacheco, F.; Cabrera, D.; Sanchez, V.; Zurita, G. Observer-biased bearing condition monitoring: Fromfault detection to multi-fault classification. *Eng. Appl. Artif. Intell.* **2016**, *50*, 287–301. [CrossRef]
31. Ali, J.B.; Saidi, L.; Mouelhi, A.; Chebel-Morello, B.; Fnaiech, F. Linear feature selection and classification using PNN and SFAM neural networks for a nearly online diagnosis of bearing naturally progressing degradations. *Eng. Appl. Artif. Intell.* **2015**, *42*, 67–81.

32. Saidi, L.; Ali, J.B.; Fnaiech, F. Application of higher order spectral features and support vector machines for bearing faults classification. *ISA Trans.* **2015**, *54*, 193–206. [CrossRef] [PubMed]
33. Huang, T.; Fu, S.; Feng, H.; Kuang, J. Bearing fault diagnosis based on shallow multi-scale convolutional neural network with attention. *Energies* **2019**, *12*, 3937. [CrossRef]
34. Wan, L.; Li, H.; Chen, Y.; Li, C. Rolling bearing fault prediction method based on QPSO-BP neural network and dempster–shafer evidence theory. *Energies* **2020**, *13*, 1094. [CrossRef]
35. Do Nascimento, C.F.; de Oliveira, A.A., Jr.; Goedtel, A.; Serni, P.J.A. Harmonic identification using parallel neural networks in single-phase systems. *Appl. Soft Comput.* **2011**, *11*, 2178–2185. [CrossRef]
36. Godoy, W.F.; da Silva, I.N.; Goedtel, A.; Palácios, R.H.C.; Lopes, T.D. Application of intelligent tools to detect and classify broken rotor bars in three-phase induction motors fed by an inverter. *IET Electr. Power Appl.* **2016**, *10*, 430–439. [CrossRef]
37. Haykin, S.O. *Neural Networks and Learning Machines, Hardcover*, 3rd ed.; Prentice Hall: Upper Saddle River, NJ, USA, 2008.
38. Lopes, T.D.; Goedtel, A.; Palácios, R.H.C.; Godoy, W.F.; de Souza, R.M. Bearing fault identification of three-phase induction motors bases on two current sensor strategy. *Soft Comput.* **2017**, *21*, 6673–6685. [CrossRef]
39. Drif, M.; Cardoso, A. Stator fault diagnostics in squirrel cage three-phase induction motor drives using the instantaneous active and reactive power signature analyses. *IEEE Trans. Ind. Inform.* **2014**, *10*, 1348–1360. [CrossRef]
40. Barendse, P.; Pillay, P. The detection of unbalanced faults in inverter-fed induction machines. In Proceedings of the IEEE International Symposium on Diagnostics for Electric Machines, Power Electronics and Drives, Cracow, Poland, 6 September 2007; pp. 46–51.
41. Wolbank, T.; Nussbaumer, P.; Chen, H.; Macheiner, P. Monitoring of rotor-bar defects in inverter-fed induction machines at zero load and speed. *IEEE Trans. Ind. Electron.* **2011**, *58*, 1468–1478. [CrossRef]
42. Chua, T.; Tan, W.W.; Wang, Z.X.; Chang, C. Hybrid time-frequency domain analysis for inverter-fed induction motor fault detection. In Proceedings of the IEEE International Symposium on Industrial Electronics (ISIE), Bari, Italy, 4 July 2010; pp. 1633–1638.
43. Basaran, M.; Ece, D. Detection of mechanical faults in induction motors supplied with adjustable speed drives. In Proceedings of the IEEE International Electric Machines and Drives Conference (IEMDC), Miami, FL, USA, 3 May 2009; pp. 1414–1419.
44. Araújo, R.; Rodrigues, R.A.; De Paula, H.; Baccarini, L.M.R. Premature wear and recurrent bearing failures at an MIT: A case study. In Proceedings of the 9th IEEE/IAS International Conference on Industry Applications (INDUSCON), Sao Paulo, Brazil, 8 November 2010; pp. 1–6. (In Portuguese)
45. Faiz, J.; Ghorbanian, V.; Ebrahimi, B. Locating broken bars in line-start and inverter-fed induction motors using modified winding function method. *Electromagnetics* **2012**, *32*, 173–192. [CrossRef]
46. Briz, F.; Degner, M.; Guerrero, J.; Garcia, P. Stator windings fault diagnostics of induction machines operated from inverters and soft-starters using high-frequency negative-sequence currents. *IEEE Trans. Ind. Appl.* **2009**, *45*, 1637–1646. [CrossRef]
47. Seshadrinath, J.; Singh, B.; Panigrahi, B. Investigation of vibration signatures for multiple fault diagnosis in variable frequency drives using complex wavelets. *IEEE Trans. Power Electron.* **2014**, *9*, 936–945. [CrossRef]
48. Jin, X.; Yuan, F.; Chow, T.W.; Zhao, M. Weighted local and global regressive mapping: A new manifold learning method for machine fault classification. *Eng. Appl. Artif. Intell.* **2014**, *30*, 118–128. [CrossRef]
49. Liu, Z.; Cao, H.; Chen, X.; He, Z.; Shen, Z. Multi-fault classification based on wavelet SVM with PSO algorithm to analyze vibration signals from rolling element bearings. *Neurocomputing* **2013**, *99*, 399–410. [CrossRef]